Report no. changed (Mar 2006): SM-377-UU

SACLANTCEN MEMORANDUM
serial no: SM- 377

SACLANT UNDERSEA RESEARCH CENTRE REPORT

Benchmarking of SCARAB volume scattering versus OASES volume scattering

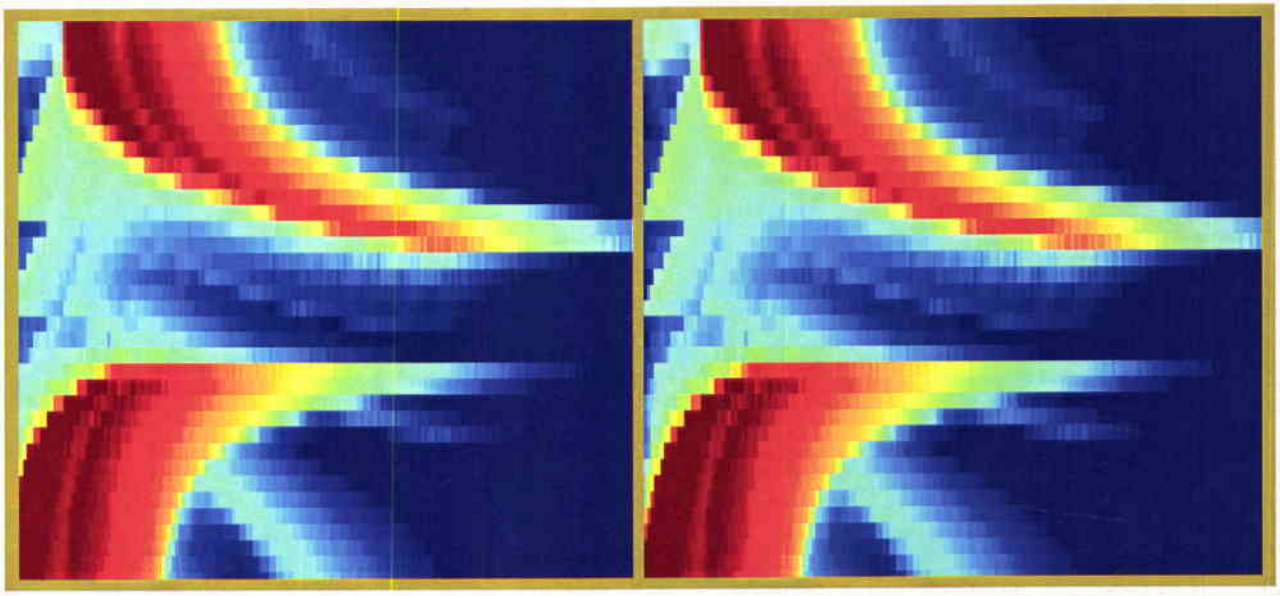

Ivar Bratberg, Kevin D. LePage, Charles Holland and Henrik Schmidt

May 2001

NORTH ATLANTIC TREATY ORGANIZATION ORGANISATION DU TRAITE DE L'ATLANTIQUE NORD

SACLANTCEN SM-377

Benchmarking of SCARAB volume scattering versus OASES volume scattering

Ivar Bratberg, Kevin LePage,
Charles Holland and Henrik Schmidt

The content of this document pertains to work performed under Project 04-D of the SACLANTCEN Programme of Work. The document has been approved for release by The Director, SACLANTCEN.

Jan L. Spoelstra
Director

intentionally blank page

Benchmarking of SCARAB volume scattering versus OASES volume scattering

Ivar Bratberg, Kevin LePage, Charles Holland and Henrik Schmidt

Executive Summary: SCARAB and OASES are acoustic models designed to estimate backscattering from marine sediments over a broad range of frequencies used for ASW and MCM. The backscattering extension to OASES provides more accurate results for fast sediments and sediments with sound speed gradients. SCARAB is benchmarked against the new OASES model and limitations are identified.

intentionally blank page

Benchmarking of SCARAB volume scattering versus OASES volume scattering

Ivar Bratberg, Kevin LePage, Charles Holland and Henrik Schmidt

Abstract: OASES uses wavenumber integration to solve for the backscattered pressure caused by sound speed and density inhomogeneity scatterers in the sediment; SCARAB uses a ray path technique to find the backscattered intensity. This report compares the two models for a variety of sediment backscattering scenarios and identifies situations where the accuracy of SCARAB is compromised.

Keywords: SCARAB ◦ OASES ◦ backscattering

Contents

1

Introduction

OASES and SCARAB are two programs used to find the propagation of sound in horizontally stratified media. Studies of important properties of sea, sediments and basements, have demonstrated that the assumption of homogeneous properties at the same depth gives a realistic description of the environment and reduces the scale of the problem.

Assuming a constant gradient of the square of the index of refraction in each layer in conjunction with homogeneous density in the layer, OASES solves the wave equation exactly for each layer [1]. After solving for all the layers, a global matrix equation is set up to solve boundary conditions on the borders between the layers.

Given the distributions for speed and density, OASES makes realizations and treats the inhomogeneities as virtual sources. The virtual source strength depends, due to the perturbation theory used, on the incoming field and the realizations of the distributions of the inhomogeneities [2]. There is no secondary scattering, which means that the sound is scattered only once from a given scattering sediment inhomogeneity.

SCARAB [3] uses a ray trace method ([4]), which traces different ray paths of from the source to the receiver. The main advantage of SCARAB is that it is fast; the main disadvantage is that under certain conditions it does not calculate the field correctly.

In OASES the pressure is calculated, whereas in SCARAB the intensity is calculated. As the pressure has phase information, we obtain an interference pattern in OASES but not in SCARAB. The ensemble averaged results from OASES are therefore plotted to facilitate comparison.

In the report we address the following main themes:

- Benchmarking two-way transmission loss of SCARAB against OASES.
- Modification of scatterer distribution in SCARAB from a Yamamoto to a Turgut representation.
- Analyzing the consistency between OASES and SCARAB TL predictions.

- Comparison of performance of the scattering modules.
- Benchmarking the scattering codes for a variety of scattering scenarios.

2

Transmission loss

To ensure that the transmission loss to scatterers in the sediment is the same for OASES and SCARAB, we must compare the TL in the sediment added to TL from the sediment to the source, see (Fig. 1). OASES measures the TL as

$$TL = -20 \log \left| \frac{P_1}{P_o} \right| \tag{1}$$

SCARAB measures TL in terms of

$$TL = -20 \log \left| \frac{P_1 \rho_0 c_0}{P_o \rho_1 c_1} \right| \tag{2}$$

2.1 Monostatic case

The environment has two layers, an upper halfspace of water which has no loss, and an acoustic halfspace of sediment. The models are used to calculate the TL at 500 Hz from a source 28 m above the sediment-water interface to a vertical array of receivers in the bottom at 700 m range and *vice versa* (Fig. 1). Seven different cases are investigated. As basement properties are equal to the sediment properties, there are in effect only two layers, although the scatterers are only situated in the sediment.

The seven cases shown in Table 1 were designed to test features of the transmission loss and scatter modules in the OASES and SCARAB codes. Agreement between the codes for transmission loss and scattering from slow sediments, fast sediments, sediments with and without density contrasts and sediments with sound speed gradients can all be evaluated with the seven cases. In Cases 1 to 5, (Fig. 2 to Fig. 6), there is good agreement between the 2-way TL in OASES and SCARAB. In Case 6, (Fig.7), the SCARAB differs significantly from the OASES solution. In Case 6 the waves in the sediment are upward refracting, and they interfere with waves traveling downward from the water-sediment interface. OASES predicts this interference pattern; SCARAB does not. SCARAB calculates total incoherent intensity and therefore has no phase information. OASES calculates the pressure and therefore predicts interference patterns. In Case 7 we see that the results fit quite well until a certain depth.

Case Number	Density 1	Density 2	Speed 1	Speed 2
1.	1.024	1.024	1500	1455
2.	1.024	1.024	1500	1600
3.	1.024	2.0	1500	1500
4.	1.024	2.0	1500	1600
5.	1.024	1.4	1500	1455
6.	1.024	2.0	1500	1600-1700
7.	1.024	1.4	1500	1455-1555

Table 1 *The table shows the setup for the cases used for benchmarks. In all cases there is attenuation of* 0.01 dB/λ *in the sediment and basement. In all cases the source is* 28 *m above the sediment water interface. The vertical array consists of* 51 *receivers spaced at* 1 *m with the centre of the array at a height of* 25 *m above the sediment-water interface.*

In Case 7, the propagation is simulated with with the raytrace program CASS [5]. The shadow effect (upper panel of Fig. 9) starts at 600 m at a depth of 230 m and widens out in the depth dimension at longer range. The shadow zone is only significant for the deepest receivers in the sediment layer at the range of 700 m. The shadow effect results from the lack of an evanescent field in the ray trace methods. In the sediment layer there is an essentially linear sound speed gradient and as a result the rays have circular paths. In the basement there is no gradient and the rays touching the basement with a negative grazing angle (downward propagation), will be lost into the basement. Therefore the upper part of the shadow zone is well approximated by the circle shaped path having a grazing angle equal to zero at the sediment-basement interface. We have used OASES to generate a transmission loss plot of the same region, see the lower panel of Fig. 9. We can see the shadow zone as explained above as fast decay of intensity into the shadow zone.

By using Snell's law, we can find the range where a ray touches the bottom before propagating upwards. For Case 7 we find the incident grazing angle in the water as

$$\theta_w = \arccos \frac{c_w}{c_b} = \arccos \frac{1500}{1555} = 15.28^\circ. \tag{3}$$

For a source height of 28 m above the sediment-water interface, this corresponds to a range in water before hitting the sea floor of

$$r_w = \frac{Z_b - Z_s}{\tan \theta_w} = \frac{28}{\tan 15.28^\circ} = 102.5 \text{ m}. \tag{4}$$

For a linear sound speed gradient the sound will propagate along a circular ray path in the sediment. Thus in this case it is possible to calculate the range for the deepest diving ray propagating in the sediment,

$$r_{s0} = \sin \theta_{s0} R = 548.6\text{m}, \tag{5}$$

where

$$\theta_{s0} = \arccos \frac{c(z_{top})}{c(z_{bottom})} = \arccos \frac{1455}{1555} = 20.7^{\circ} \tag{6}$$

and the radius of curvature is

$$R = \frac{c(z)}{g \cos \theta(z)} = 1555\text{m}, \tag{7}$$

and the gradient $g = 1s^{-1}$ This gives the total range from the source to the turning point at the bottom of the sediment layer of 650 m. At a range of 700 m from the source, this ray has a grazing angle upwards:

$$\theta_u = \arcsin \frac{700 - 650}{1555} = 1.84^{\circ} \tag{8}$$

which corresponds to an upward movement up of

$$\Delta z = (1 - \cos 1.84)R = 0.8\text{m}. \tag{9}$$

This indicates that there is less than a meter of shadow zone observed in the sediment at a range of 700 m. Ray traces of the reciprocal situation, with source at 180 m and 200 m, are shown in the upper panels of Fig. 10 and Fig. 11, with corresponding contour plots shown in the lower panels of these figures.

¿From these results it may be concluded that SCARAB fails to find the rays after their turning point, and thus the disagreement in the two way TL is not caused by a shadow zone.

2.2 Conclusion for TL 700 m

The two models give satisfactory results for the isovelocity cases, but not for the gradient case. This is due to a problem in SCARAB caused by its failure to include rays having a turning point deeper than the maximum receiver depth. This means that in later volume scattering comparisons between SCARAB and OASES, SCARAB is expected to give incorrect results for instances and beams when the bulk of the contributing scatterers have been ensonified by upward propagating waves. There is better coincidence between the two simulators for slow bottoms than for fast bottoms, (Fig. 12). For angles near the critical, the angular resolution of the ray trace in SCARAB becomes very low for large ranges. It is anticipated that further tuning of the ray trace algorithm in SCARAB will eliminate this difficulty. It is also anticipated that SCARAB may be modified to make better agreement for Cases 6 and 7 possible.

3

Old and new version of the scattering kernel in SCARAB

We have changed the power spectrum representation in the SCARAB code from the Yamamoto [6] case to the Turgut[7, 8] case. For low wavenumbers, the Yamamoto representation gives large values. Turgut has introduced a constant to limit power spectrum values towards infinity for low values of the wavenumber. In three dimensions the Yamamoto equation has the form:

$$S_v(\mathbf{k}) = \frac{\beta \Lambda^2 B}{2\pi}(\Lambda^2 k_x^2 + \Lambda^2 k_y^2 + k_z^2)^{-(\beta+2)/2}, \tag{10}$$

where $\beta + 2$ is the spectral exponent, B is a proportionality constant, Λ is a non-dimensional ratio between an isotropic correlation length scale l_r and the vertical correlation length scale l_z, k_x and k_y are horizontal wavenumbers and k_z is the vertical wavenumber and $\mathbf{k} \equiv [k_x, k_y, k_z]$.

The Turgut equation in three dimensions has the form

$$S_v(\mathbf{k}) = \mu l_r l_y l_z \pi^{-3/2} \frac{\Gamma(m)}{\Gamma(m - 3/2)}(1 + \xi^2)^{-m}, \tag{11}$$

where in the isotropic case

$$\xi = \sqrt{l_r^2 k_r^2 + l_z^2 k_z^2}. \tag{12}$$

In Turgut's equations μ is a proportionality constant, l_x and l_y are horizontal correlation length scales which in the isotropic case give $l_r = \sqrt{l_x^2 + l_x^2} = \sqrt{l_y^2 + l_y^2}$, l_z is the vertical correlation length scale and $2m$ is the spectral exponent.

It was decided to introduce the Turgut equation in such a way that it would converge towards the Yamamoto equation for large arguments. Thus it is necessary that the spectral exponents in the two equations be the same:

$$\beta + 2 = 2m. \tag{13}$$

We rewrite the Turgut equation:

$$S_v(\mathbf{k}) = \mu l_r^2 l_z^{1-2m} \pi^{-3/2} \frac{\Gamma(m)}{\Gamma(m - 3/2)}(\frac{1}{l_z^2} + \Lambda^2 k_r^2 + k_z^2)^{-m}, \tag{14}$$

or

$$S_v(\mathbf{k}) = \mu\Lambda^2 l_z^{3-2m}\pi^{-3/2}\frac{\Gamma(m)}{\Gamma(m-3/2)}(\frac{1}{l_z^2} + \Lambda^2 k_r^2 + k_z^2)^{-m}. \tag{15}$$

This enables us to write an equation for μ given β:

$$(2m-2)B\sqrt{\pi} = 2\mu l_z^{3-2m}\frac{\Gamma(m)}{\Gamma(m-3/2)}, \tag{16}$$

or

$$\mu = Bl_z^{2m-3m}\sqrt{\pi}(m-1)\frac{\Gamma(m-3/2)}{\Gamma(m)}. \tag{17}$$

For the values of $m = 1.75$ we obtain

$$\mu = \frac{B\sqrt{l_z}}{0.1907} \tag{18}$$

The old and the new version of the scattering kernels in SCARAB were tested (Figs. 13-16). There are only slight differences between the SCARAB predictions of the time-angle evolution of sediment scattering for these two spectral representations of the scatterer distributions over a broad range of frequencies of interest.

4

Theory versus SCARAB for Case 8

Case 8 compares SCARAB output with a simple calculation of the backscattered intensity from a sediment layer with background properties identical to the water column. The environment is of uniform density and speed. The incoming intensity is calculated as a function of time. We use the definition of differential scattering strength to express the scattered intensity at a certain distance r from the scatterer

$$I_s(t,\theta) = \frac{SS(\theta)V(t)I_0}{r^2}, \tag{19}$$

where SS is the scattering cross section of the inhomogeneities per unit volume as a function of grazing angle θ, I_o is the incident intensity, r is the distance from the source/receiver to the scattering volume V, and the size of the scattering volume is

$$V(t) = 2\pi g D c\tau/2,$$

where the pulse length τ is one over the bandwidth $\triangle\Omega$ in Hz

$$\tau = \frac{1}{\triangle\Omega}. \tag{20}$$

¿From Yamamoto [6], we have a closed form of expression for the scattering cross section of sediment volume inhomogeneities as a function of frequency, grazing ange and the inhomogeneity power spectrum P_μ

$$SS(\theta) \approx 2\pi \left(1 - e_i e_s \gamma\right)^2 k_0^4 P_\mu(\Delta k), \tag{21}$$

where γ is one-half the ratio between the rms non-dimensional density perturbation $\triangle\rho/\rho_b$ and the rms non-dimensional sound speed perturbation $\triangle c/c_b$

$$\gamma = 0.5 \triangle \rho\, c_b / \triangle c\, \rho_b.$$

The scattered intensity is then given by

$$I_s(t,\theta) = \frac{2\pi(1+2\gamma)^2 k_0^4 P_\mu(-2\vec{e}_{incident}) 2\pi\sqrt{r^2 - (H + D/2)^2} D \frac{c\tau}{2} 10^{SL/10}}{r^4}. \tag{22}$$

For the Turgut type power spectrum we have

$$P_\mu = \mu l_r^2 l_z \pi^{-3/2} \frac{\Gamma(1.75)}{\Gamma(0.25)} (1 + \xi^2)^{-1.75}, \tag{23}$$

where

$$\xi^2 = k_z^2 l_z^2 + k_r^2 l_r^2. \tag{24}$$

The results, which verify that SCARAB is close to the expected intensity as a function of time are shown in Figs. 17 and 18.

5

Simulations of Cases 1 through 7 with SCARAB and OASES

In Figs. 19-32 we present the results of comparison between SCARAB and OASES for the seven cases shown in Table 1. For each case there are three figures. There are two plots of the backscattered field vs angle and time, one each for SCARAB and OASES and one backscattered intensity plot showing predictions from the two codes superimposed for a monostatic source-receiver configuration.

For fast bottoms, Cases 2, 4 and 6, we see a split in the intensity picture for small negative grazing angles, due to the existence of a critical angle. The secondary branch of intensity in OASES is due to near zero degree propagation and return, a kind of forced scattering of evanescent waves from the sound field close to the interface.

The values in the OASES simulations fluctuate about the SCARAB values, due to Monte-Carlo averaging of only 16 scattered pressure realizations. To have a better impression of intensity levels, an increased number of averages would be required. The good agreement between the two codes for slow bottoms deteriorates for fast bottoms and bottoms with gradients. In these cases, the OASES solution is superior to the SCARAB solution due to the deficiencies in the field calculation in SCARAB identified in Section 2.

6

Conclusion

Results from simulations of simple environments for SCARAB and for OASES are presented. Incoming intensity is shown as a function of time and angle. The results agree for simple slow bottoms, but for fast bottoms, or bottoms with gradients, the OASES solution is superior. In SCARAB there are two main limitations:

- The calculation of rays after they reach the turning point.
- The lack of calculation of scattering from evanescent waves.

The first point can be remedied, the other constitutes a limitation for the power spectrum representation of scatterers.

7 Acknowledgements

Ivar Bratberg would like to thank many people at the SACLANT Centre for helping him during his tenure as a Summer Research Assistant. Most of all he would like to thank Finn Jensen, Carlo Ferla, Giovanna Martinelli, Cinzia Isoppo and Peter Nielsen.

References

[1] Schmidt, H. SAFARI: Seismo-acoustic fast field algorithm for range independent environments. User's guide, SACLANTCEN SR–113. La Spezia, Italy, SACLANT Undersea Research Centre, 1988.

[2] Lepage K.D., Schmidt, H. Spectral integral representations of monostatic scattering from three dimensional distributions of sediment volume inhomogeneities, SACLANTCEN SM-376. La Spezia, Italy, SACLANT Undersea Research Centre, 2000.

[3] Rogers A., Holland, C. SCARAB version 1.01, Users manual. Planning Systems Incorporated, 1997.

[4] Jensen, F.B., Kuperman, W.A., Porter, M.B., Schmidt, H. Computational Ocean Acoustics, 2000.

[5] Weinberg, H., Keenan, R.E. Gaussian ray bundles for modeling high-frequency propagation loss under shallow water conditions. *Journal of the Acoustical Society of America* **100**, 1996:1421–1431.

[6] Yamamoto, T. Acoustic scattering in the ocean from velocity and density fluctuations in the sediments. *Journal of the Acoustical Society of America* **99**, 1996:866–879.

[7] Turgut, A. Inversion of bottom/subbottom statistical parameters from acoustic backscatter data. *Journal of the Acoustical Society of America* **102**, 1997:833–852.

[8] Goff, J.A., Jordan, T.H. Stochastic modeling of seafloor morphology: inversion of Sea Beam data for second order statistics. *Journal of Geophysical Research* **93**, 1988:13589–13608.

8 Figures

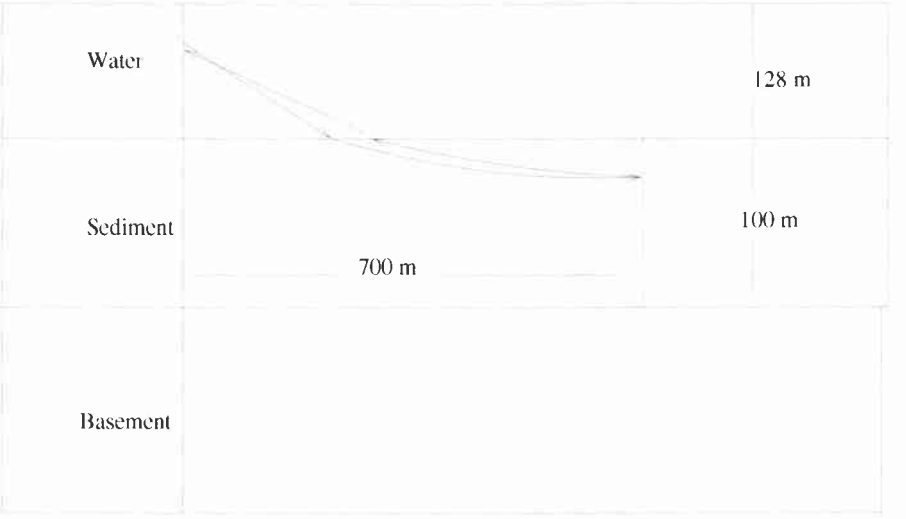

Figure 1 *Calculation of 2-way transmission loss. We calculate the TL for a ray from the source* 28 *m above the sediment-water interface to an array of receivers in the sediment at a range of* 700 *m from the source. We also calculate the TL the opposite direction and add them to obtain the 2-way TL.*

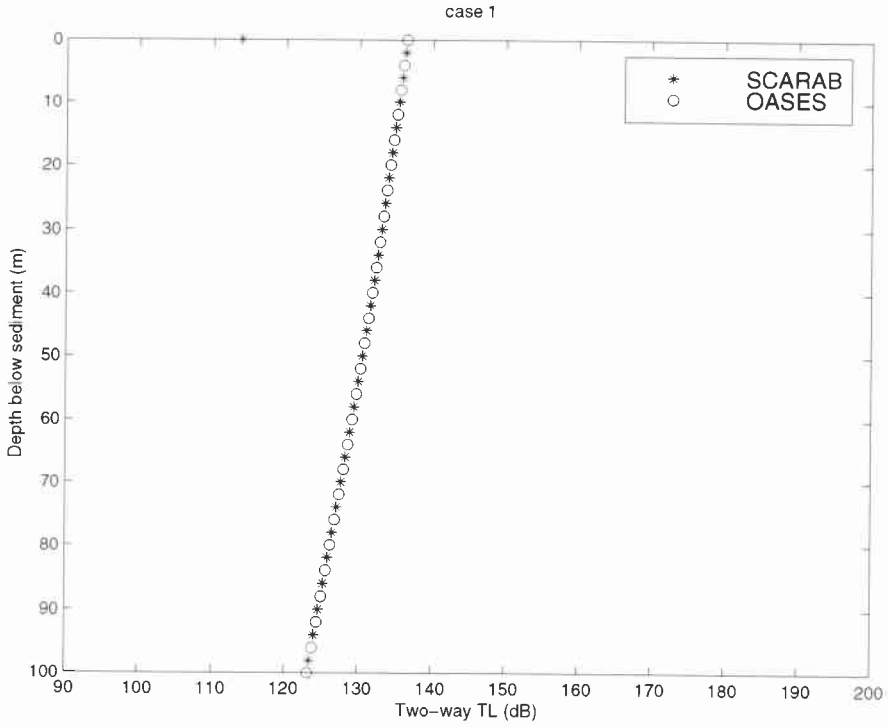

Figure 2 *Case 1, a slow bottom,* $c_b = 1455$ m/s, $\rho_b = 1.024$ g/cm^3, *where the incident rays will increase their grazing angle coming into the bottom. There is no critical angle.*

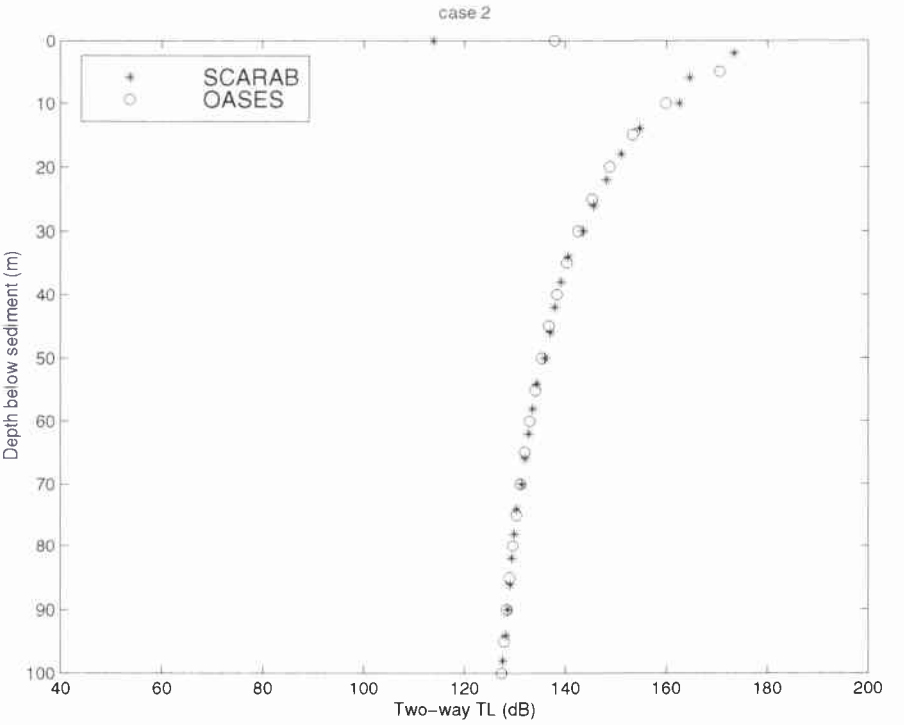

Figure 3 *Case 2, a fast bottom,* $c_b = 1600$ m/s, $\rho_b = 1.024$ g/cm^3, *where the incident rays will decrease their grazing angle coming into the bottom. There is a critical angle* $\theta_c = \arccos(1500/1600) = 20.4°$, *and we can see that for small grazing angles, there are some deviations between SCARAB and OASES.*

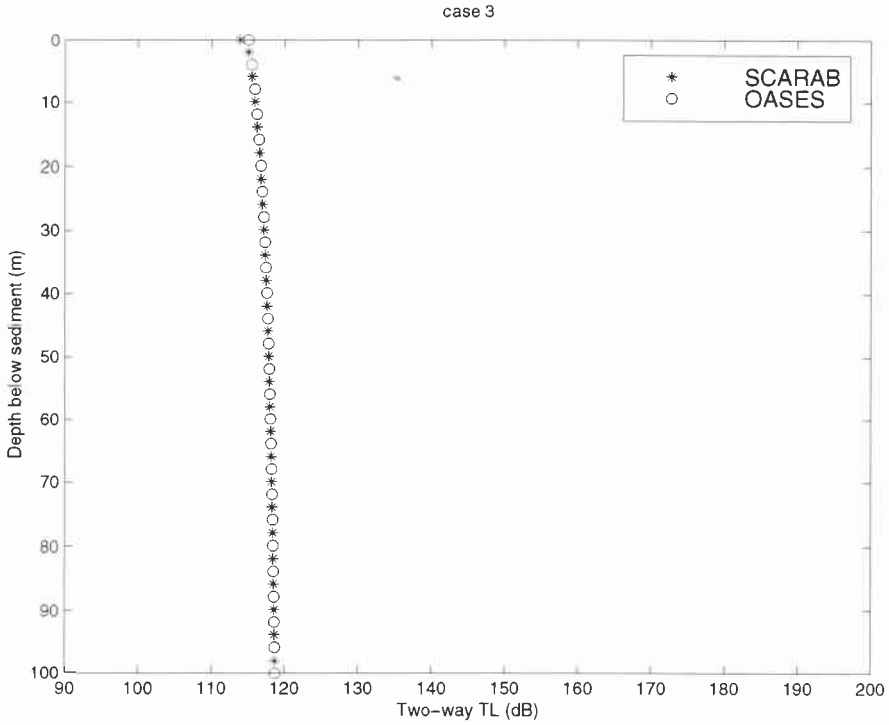

Figure 4 *Case 3, a dense bottom,* $\rho_b = 2.0$ g/cm^3, $c_b = 1500$ m/s, *there is no change in the angle of the ray and good agreement between SCARAB and OASES at all depths.*

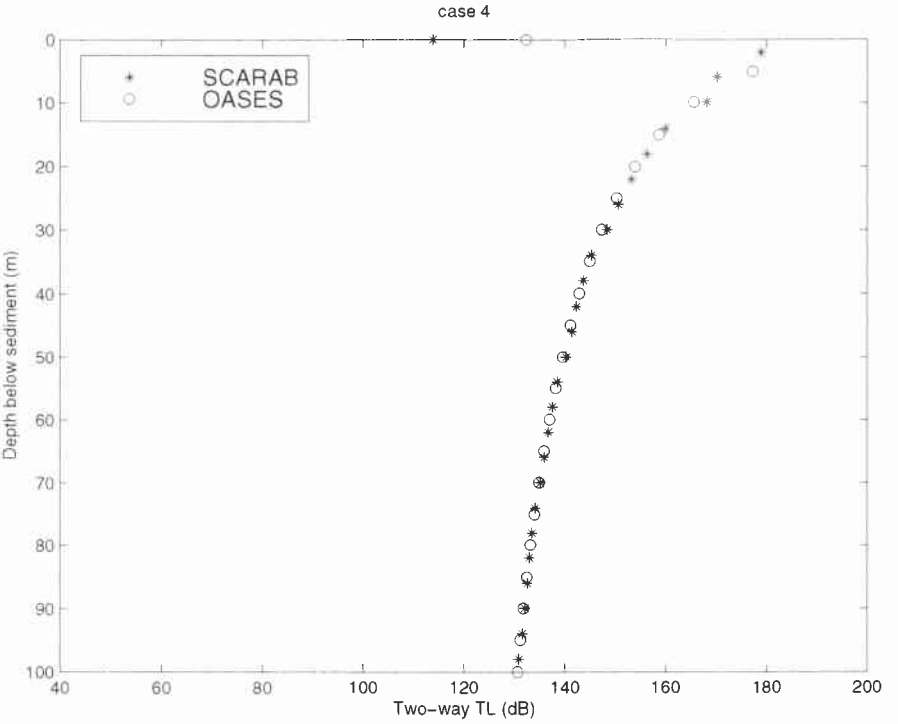

Figure 5 *Case 4, a dense and fast bottom* $\rho_b = 2.0\ \mathrm{g/cm^3}, \mathrm{c_b} = 1600\ \mathrm{m/s}$, *where the incident rays will decrease their grazing angle coming into the bottom. There exists a critical angle of* 20.4°. *There is good agreement for the deep region of the sediment but not for the shallower part. This problem is discussed in the text.*

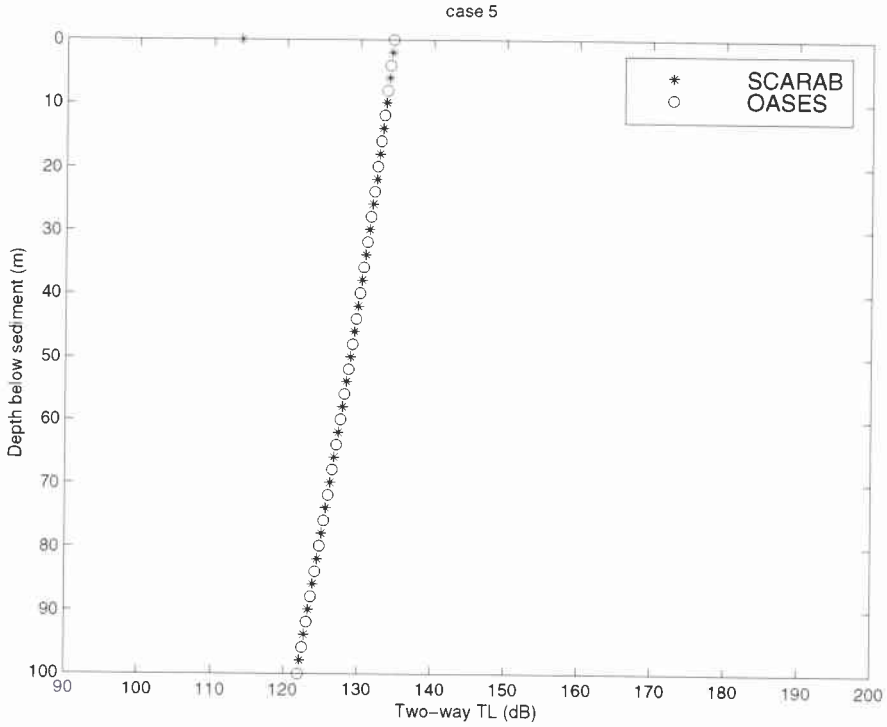

Figure 6 *Case 5, slow bottom,* $\rho_b = 1.4\ \mathrm{g/cm^3}, \mathrm{c_b} = 1400\ m/s$, *where the incident rays will increase their grazing angle coming into the bottom. There is no critical angle.*

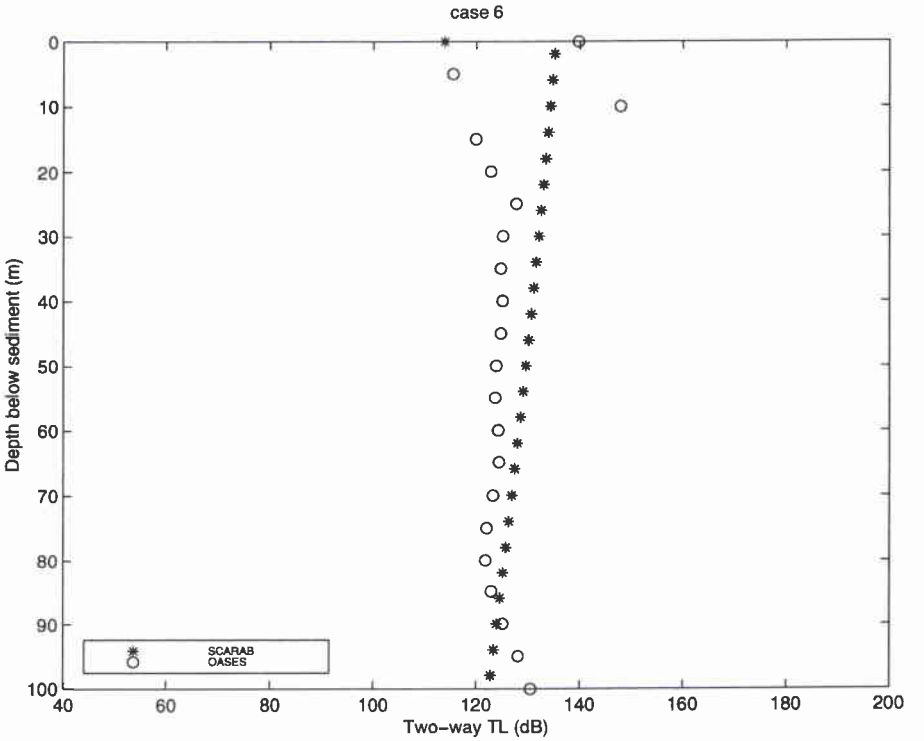

Figure 7 *Case 6, a hard bottom with a linear speed gradient* $g = 1s^{-1}, c(0) = 1600$ m/s, $\rho_b = 2.0$ g/cm^3 *where the incident rays will decrease their grazing angle coming into the bottom. OASES results show an interference behavior near the sediment-water interface. This is due to the coherent addition of the evanescent and upward refracted waves in the sediment. SCARAB does not include evanescent fields and it does not calculate interference patterns in any case since it calculates the field in terms of incoherent intensity.*

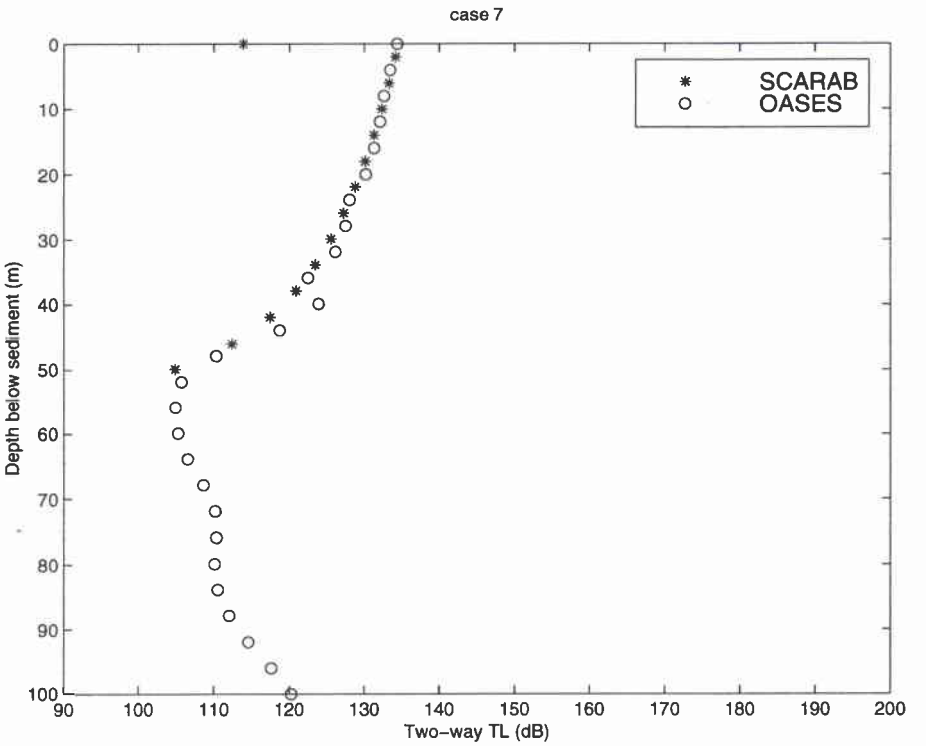

Figure 8 *Case 7, a bottom with a linear speed gradient* $g = 1s^{-1}, c(0) = 1455$ m/s, $\rho_b = 1.4$ g/cm^3. *We can see that SCARAB does not find the solution for depths greater than around 50 m. SCARAB only finds the rays whos turning point is at a shorter range and at a deeper depth than the receiver. This is confirmed by calculations whichs shows that ray paths having their turning points deeper than 50 m in the sediment, has a corresponding range for the turning point less than 700 m.*

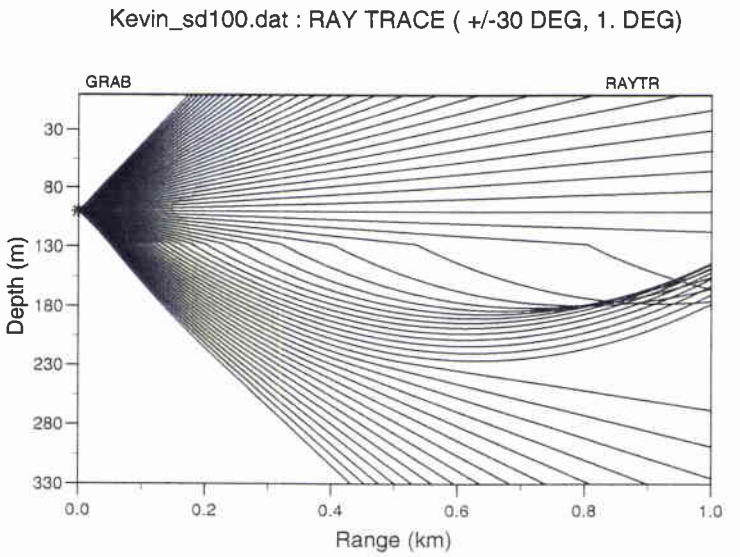

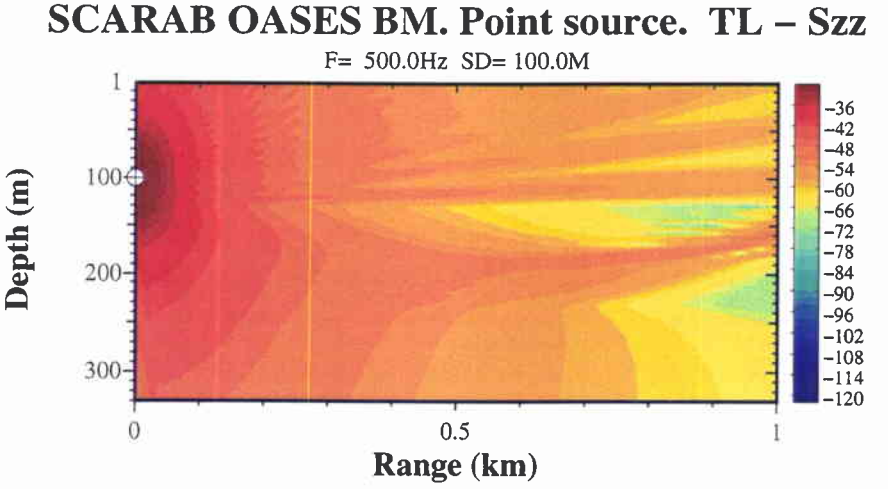

Figure 9 *Case 7, Upper figure: CASS ray tracing, source at* 100 *m, we can see that there is almost no shadow effect at the range of* 700 *m. Lower figure: OASES TL contour plot of Case 7. The shadow zone was found to start at range around* 600 *m and depth* 230 *m, see Fig. 9. For larger ranges, it widens out in both directions along the z-axis. In the figure this fact is reflected by a strongly decreasing intensity in the same area.*

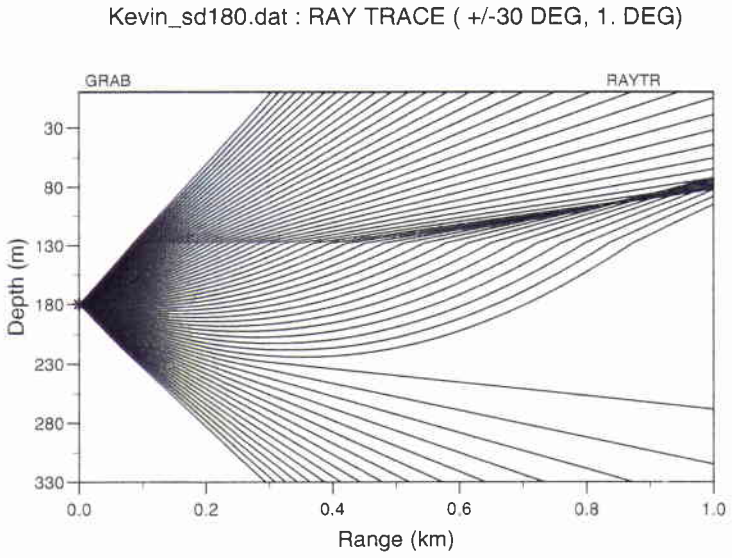

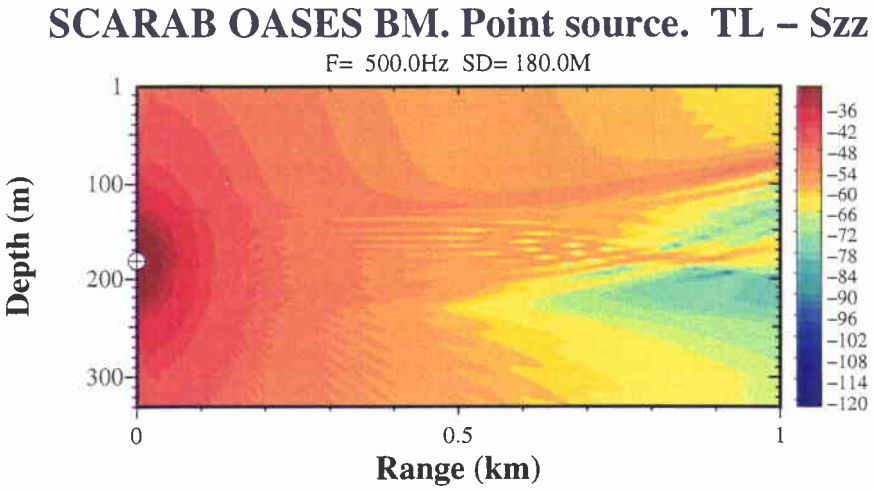

Figure 10 *Case 7, Upper figure: CASS ray tracing, source at* 180 *m. We have made this plot to see if there is a shadow zone when sound returns from the sediment column at* 700 *m range and back to the receiver at* 100 *m depth. We see that there is no shadow zone at range* 700 *m and depth* 100 *m in the water. Lower figure: OASES TL contour plot of Case 7, source at* 180 *m. Comparing with the ray trace, we can recognize the shadow zone, starting at around* 400 *m, and then widening out mostly upwards, but it does not reach the depth of the receiver before a range over* 1 *km.*

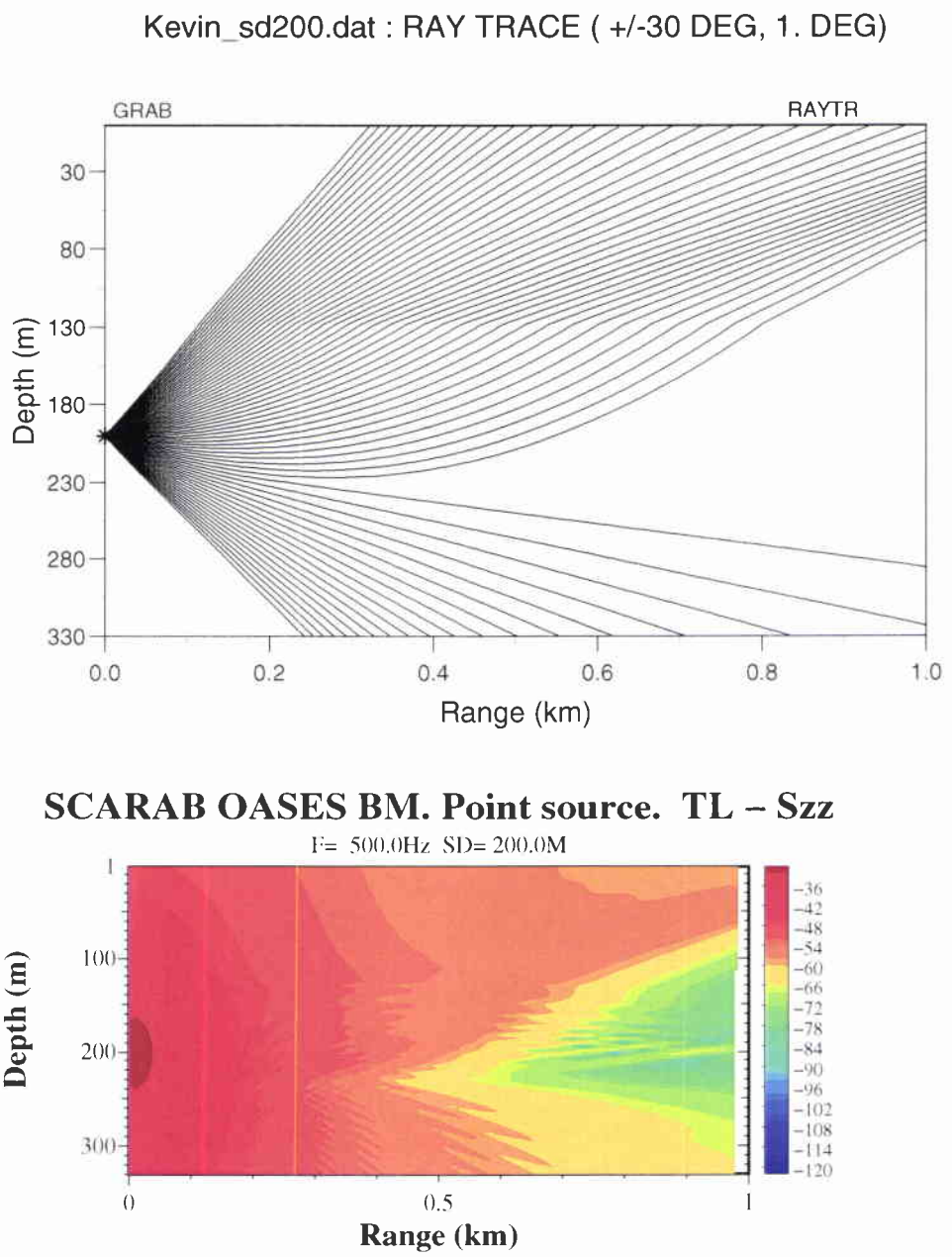

Figure 11 *Case 7, upper figure: CASS ray tracing, source at* 200 *m. We have made this plot of the same reasons as the previous figure, but at another depth. Still we see no shadow zone at a range of* 700 *m and depth of* 100 *m in the water. Lower figure: OASES TL contour plot of Case 7, source at* 200 *m. Comparing with the ray trace, we can recognize the shadow zone starting at around* 400 *m widening out mostly upwards for larger ranges, but it does not reach the depth of the receiver before reaching a range of around* 900 *m.*

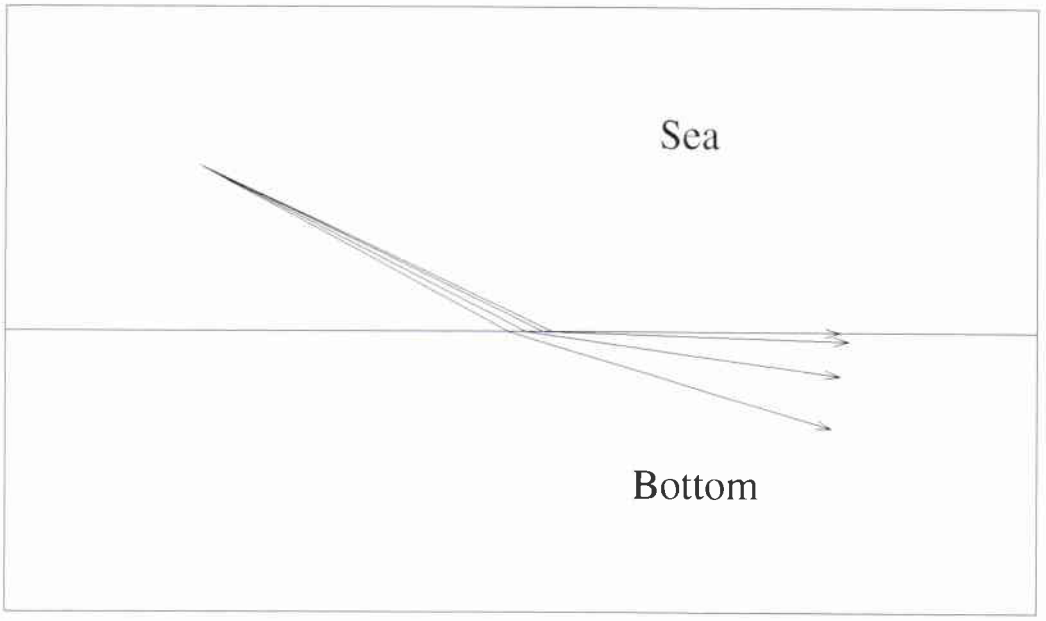

Figure 12 *Illustration of low angle resolution for a ray path finder near a critical angle. As the critical angle is approached, the grazing angle in the bottom is more poorly resolved. At large ranges from the "insertion point" of critical grazing angle energy, the ray trace program has a low resolution in the depth direction in the sediment.*

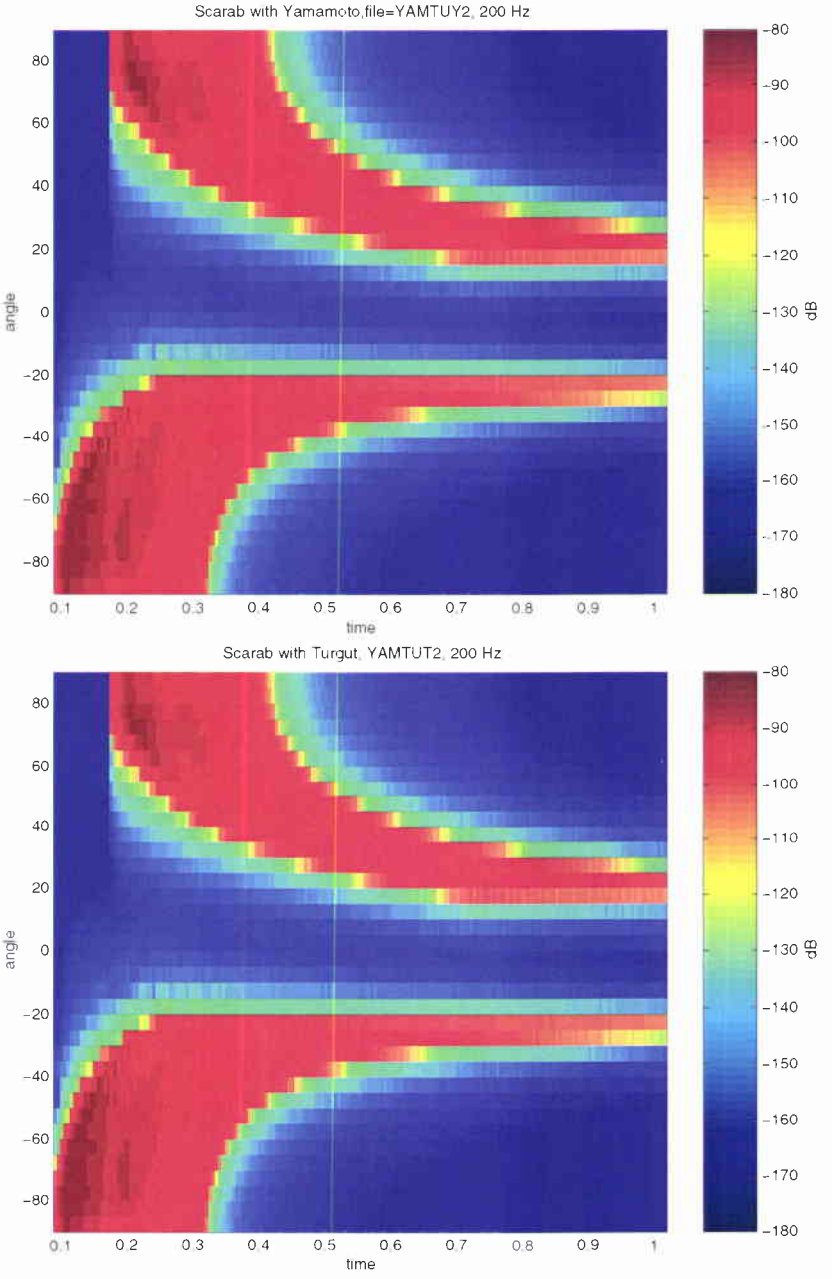

Figure 13 *Yamamoto uppermost and Turgut beneath,* $f_c = 200\text{Hz}, \text{l}_\text{r} = 5\ \text{m}, \text{l}_\text{z} = 5\ \text{m}$. *The figures look very similar.*

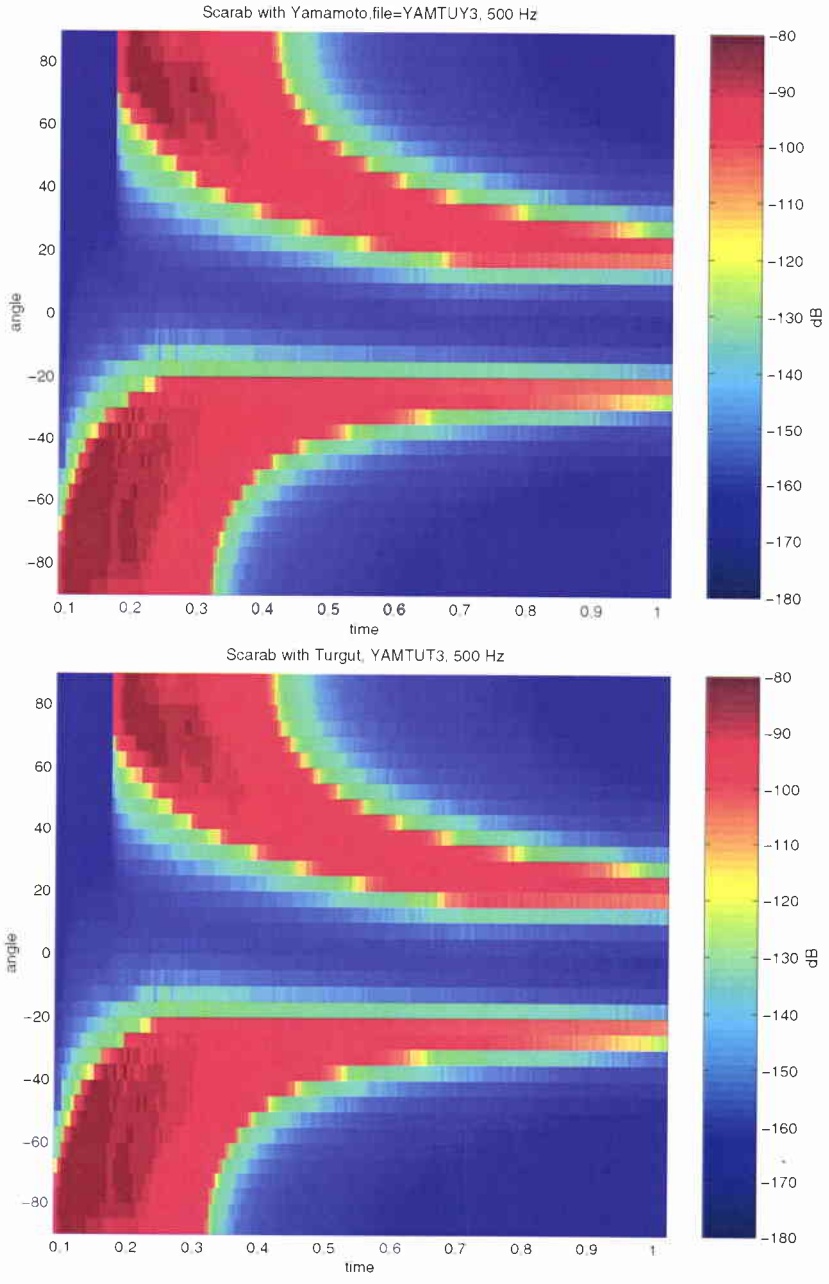

Figure 14 *Yamamoto uppermost and Turgut beneath,* $f_c = 200$ Hz, $l_r = 10$ m, $l_z = 5$ m. *The figures look very similar.*

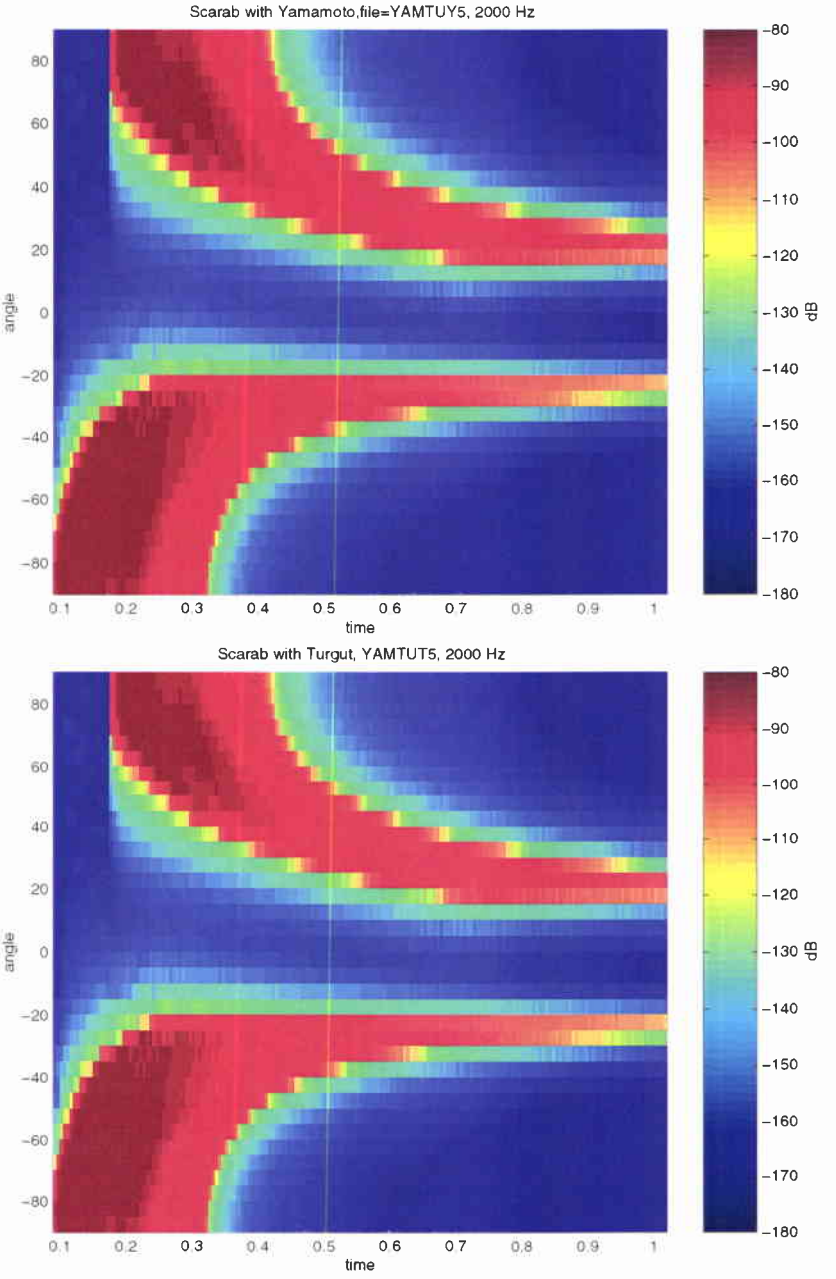

Figure 15 *Yamamoto uppermost and Turgut beneath,* $f_c = 2$ kHz, $l_r = 5$ m, $l_z = 5$ m. *The figures look very similar.*

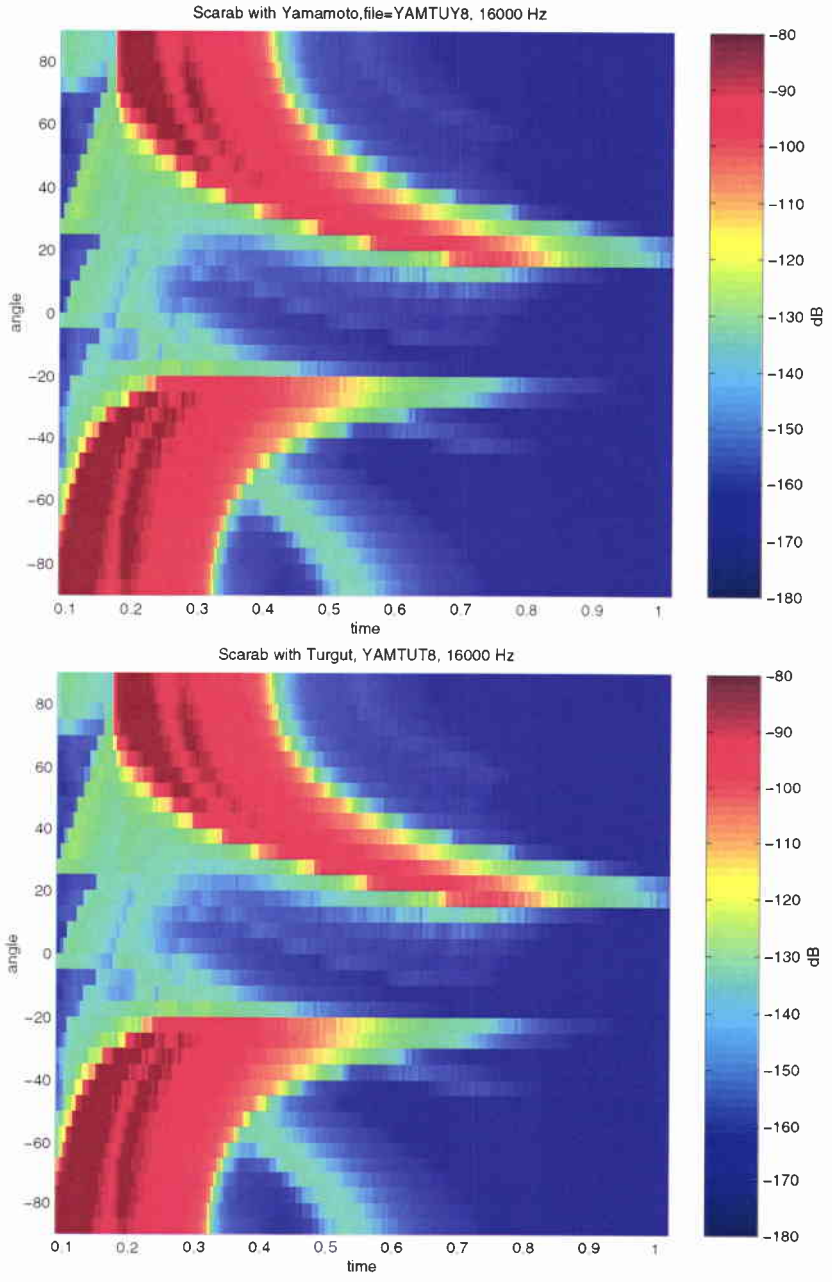

Figure 16 *Yamamoto uppermost and Turgut beneath,* $f_c = 16$ kHz, $l_r = 5$ m, $l_z = 5$ m. *The figures look very similar.*

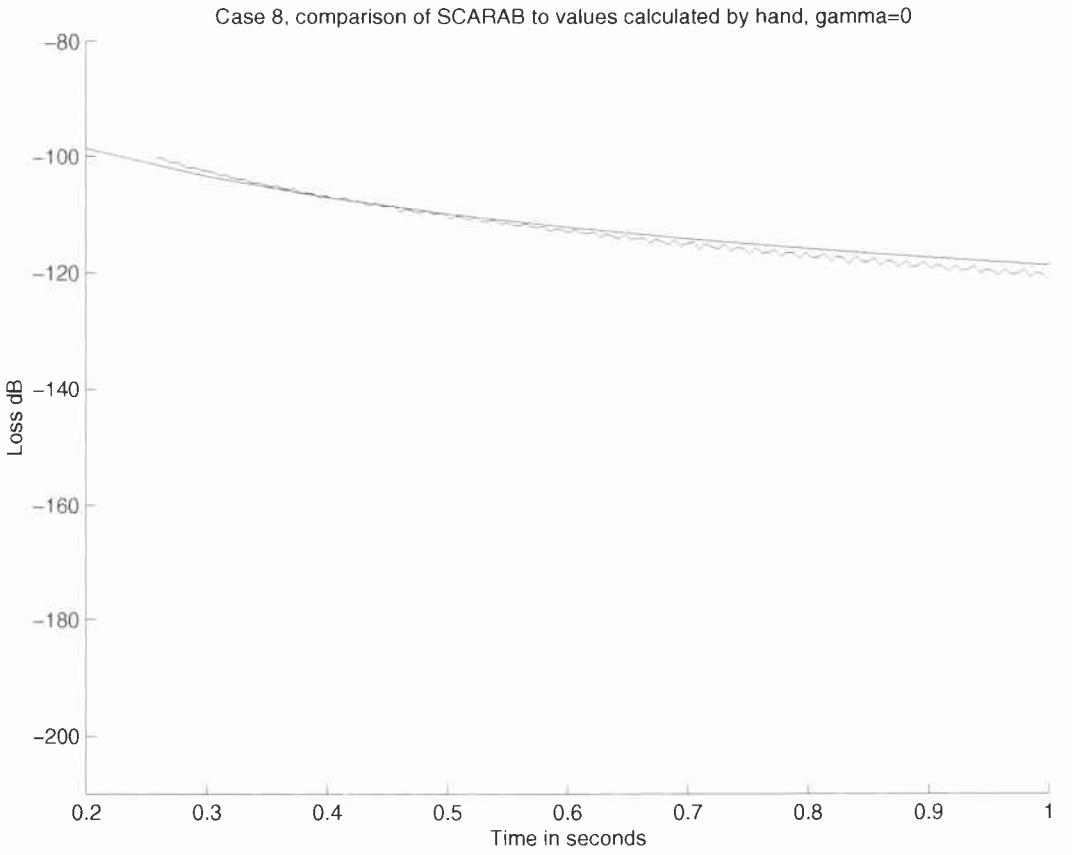

Figure 17 *Comparing the Case 8 output from SCARAB (rough curve) to the result of calculations by Eqns. 22 to 24, $\gamma = 0$ (smooth curve.)*

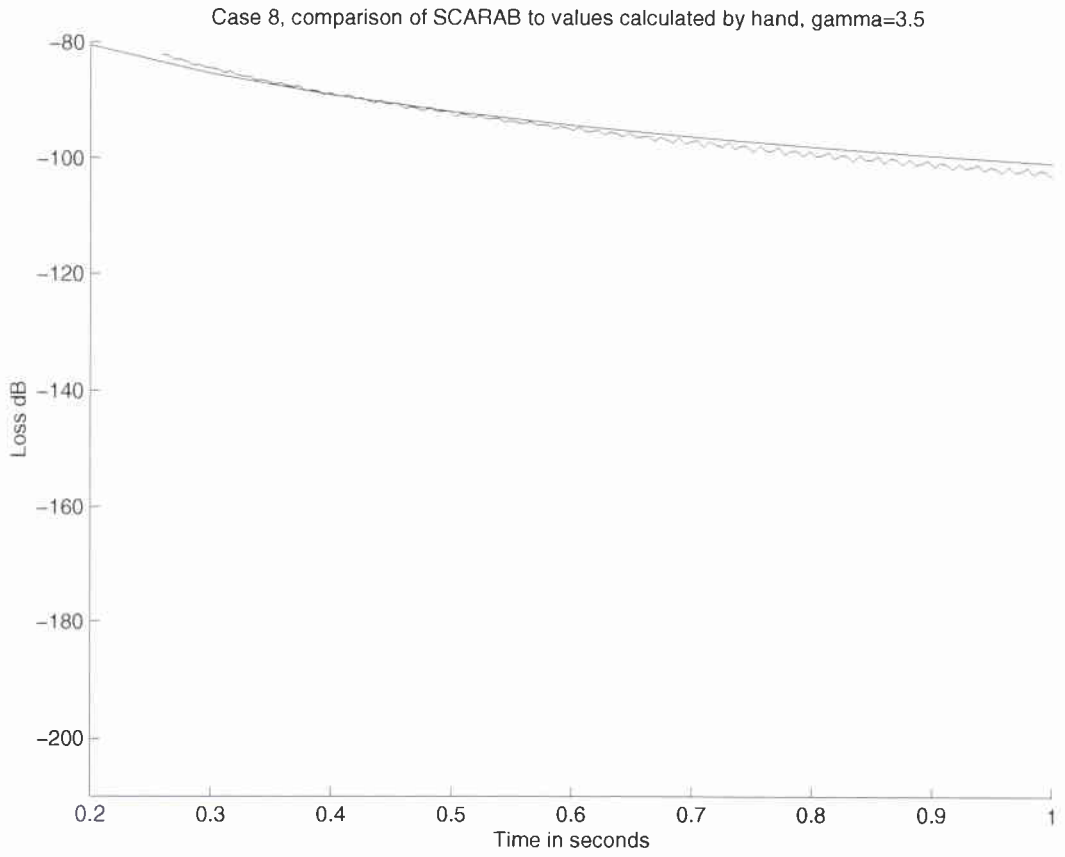

Figure 18 *Comparing Case 8 output from SCARAB (rough curve) and calculations by Eqns. 22 to 24, $\gamma = 3.5$ (smooth curve.)*

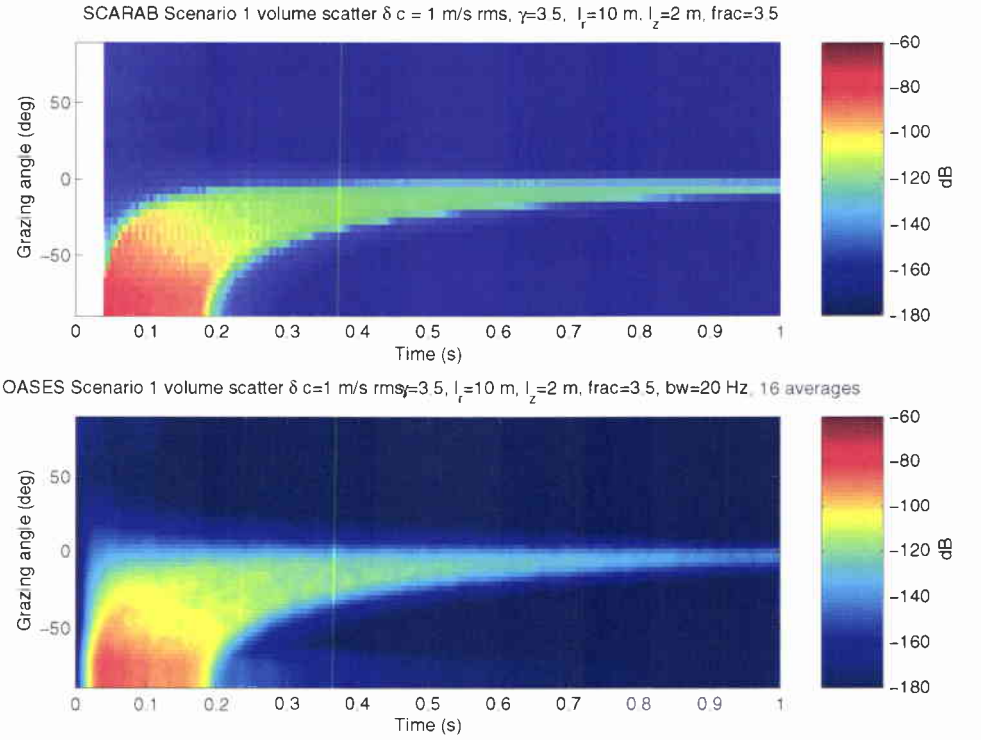

Figure 19 *Case 1, $\gamma = 3.5$, Beam-time evolution of scattered field as predicted by SCARAB (top) and OASES (bottom.)*

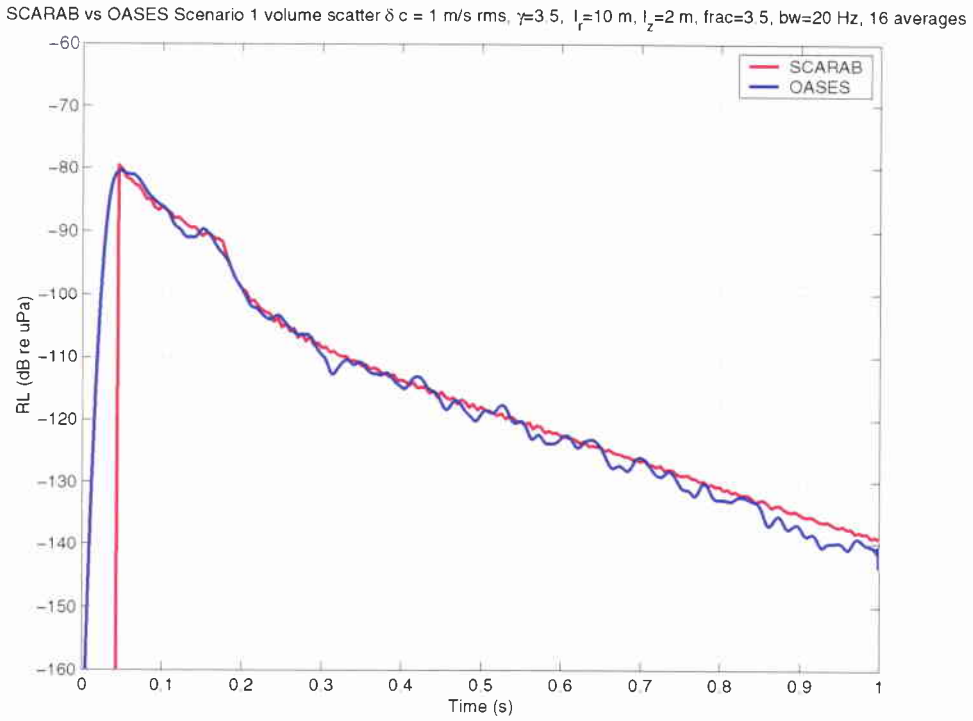

Figure 20 *Case 1, total scattered intensity as a function of time for a source/receiver combination deployed* 25 *m above the sediment-water interface (as opposed to* 28 *m in the ray trace examples in the TL section.) Predictions by SCARAB are shown in red and OASES in blue. OASES results have been ensemble averaged over* 16 *sediment scatterer realizations.*

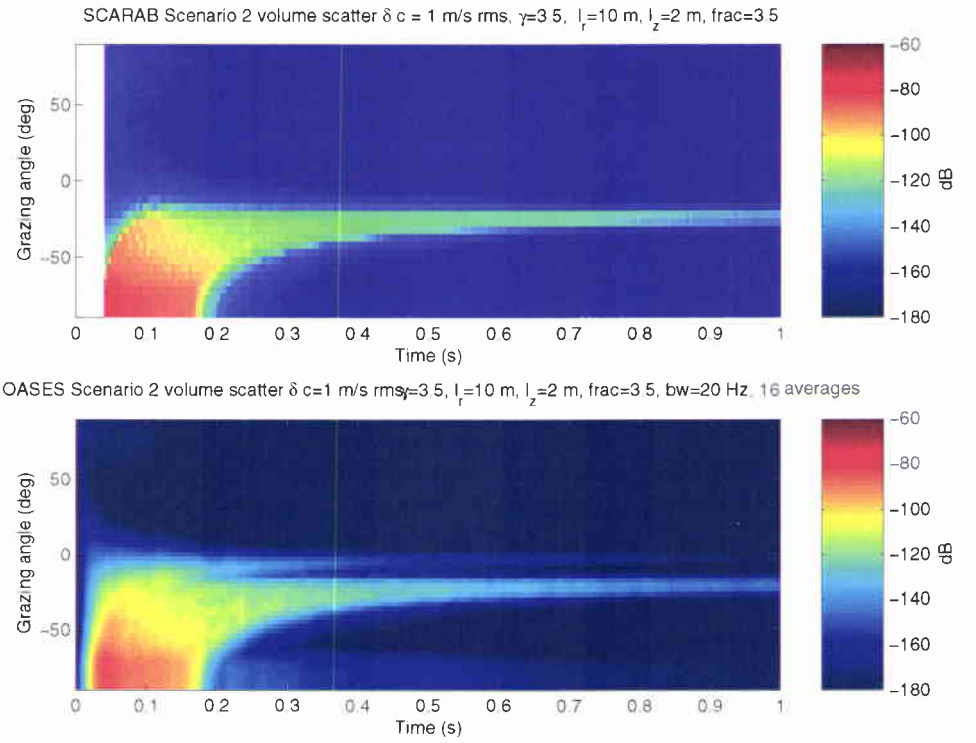

Figure 21 *Case 2, $\gamma = 3.5$, Beam-time evolution of scattered field as predicted by SCARAB (top) and OASES (bottom.) The shallow angle branch seen in the OASES results is due to evanescent forcing of the sediment volume inhomogeneities near the sediment-water interface. This type of scattering mechanism is not included in SCARAB.*

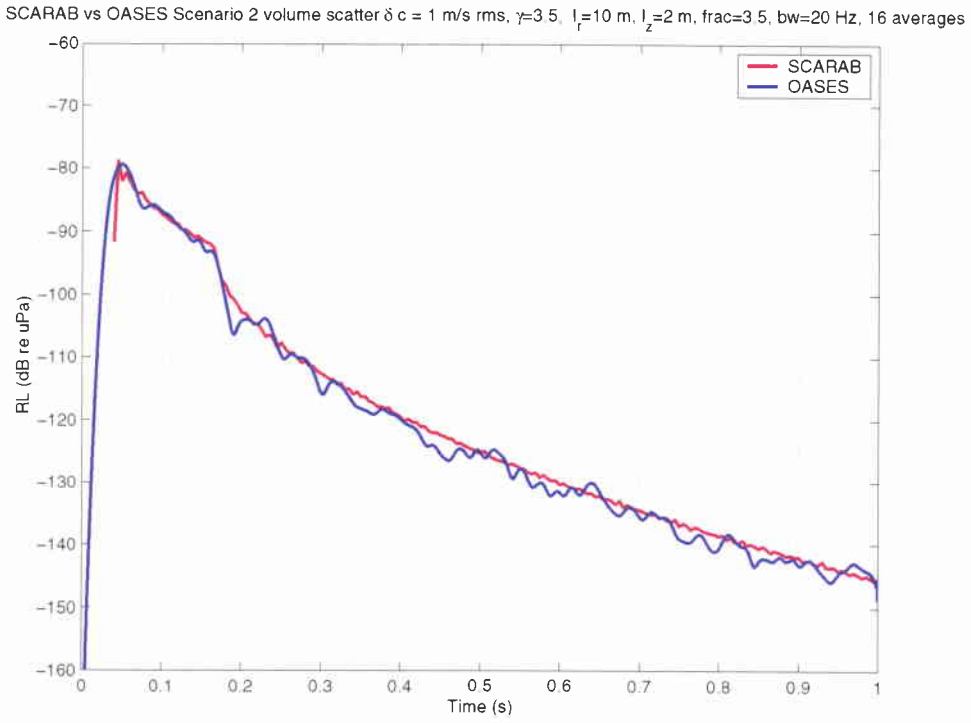

Figure 22 *Case 2, total scattered intensity as a function of time for a source/receiver combination deployed 25 m above the sediment-water interface. Predictions by SCARAB are shown in red and OASES in blue. Although the forced inhomogeneous excitation of the scatterers is neglected in the SCARAB calculation, very good agreement between the single phone levels for the two codes is still observed. This is seen to depend on the level of attenuation in the background sediment, see [7].*

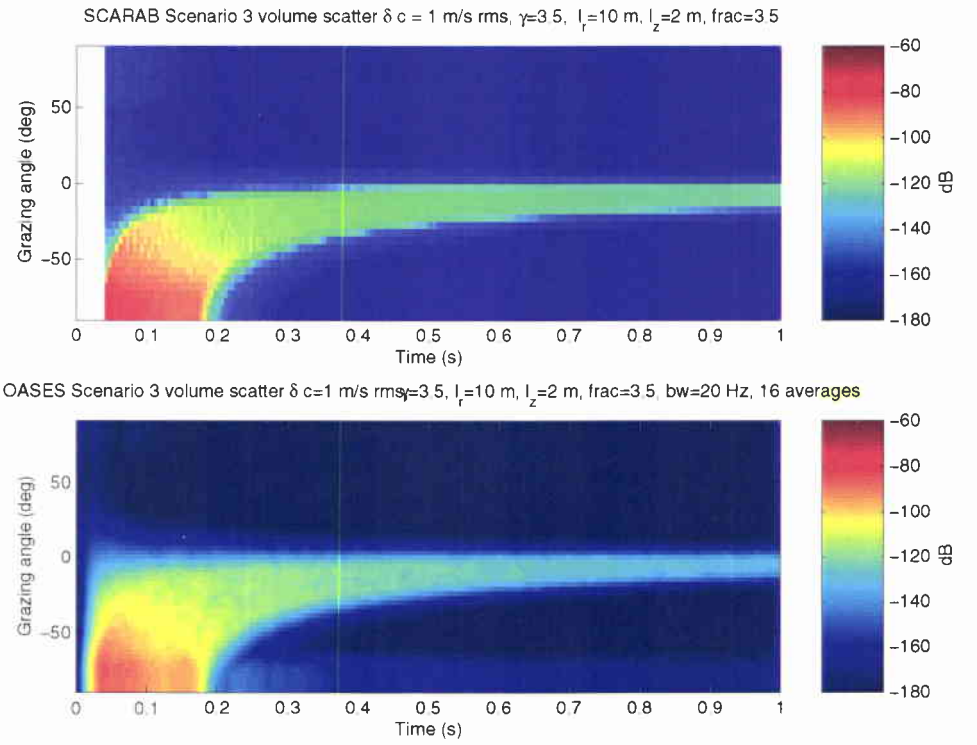

Figure 23 *Case 3, $\gamma = 3.5$, Beam-time evolution of scattered field as predicted by SCARAB (top) and OASES (bottom.)*

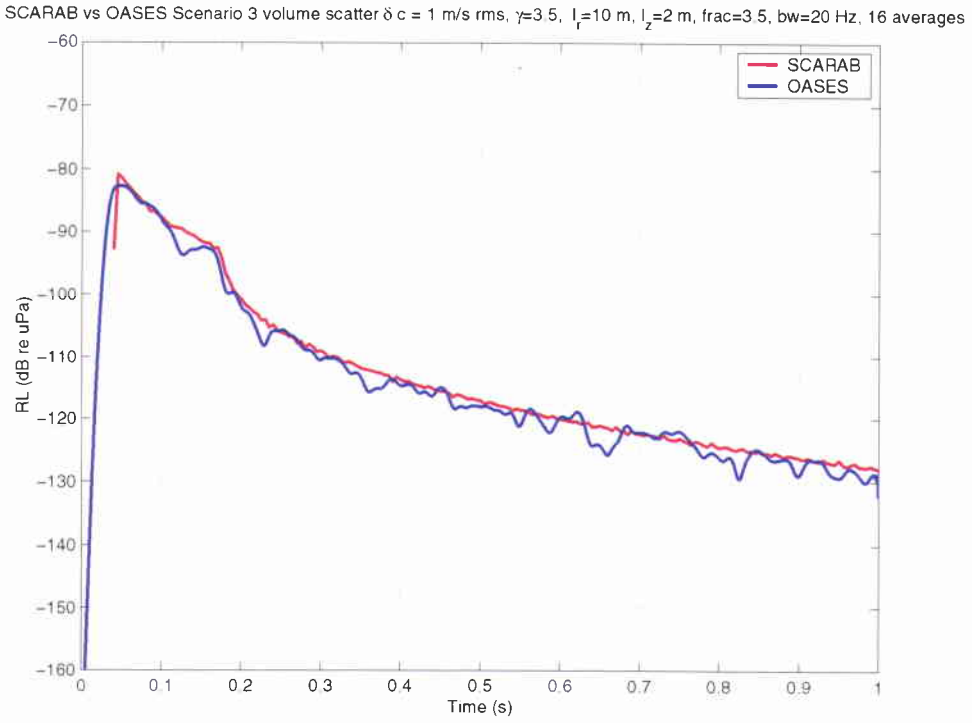

Figure 24 *Case 3, total scattered intensity as a function of time for a source/receiver combination deployed* 25 *m above the sediment-water interface. Predictions by SCARAB are shown in red and OASES in blue. OASES results have been ensemble averaged over* 16 *sediment scatterer realizations.*

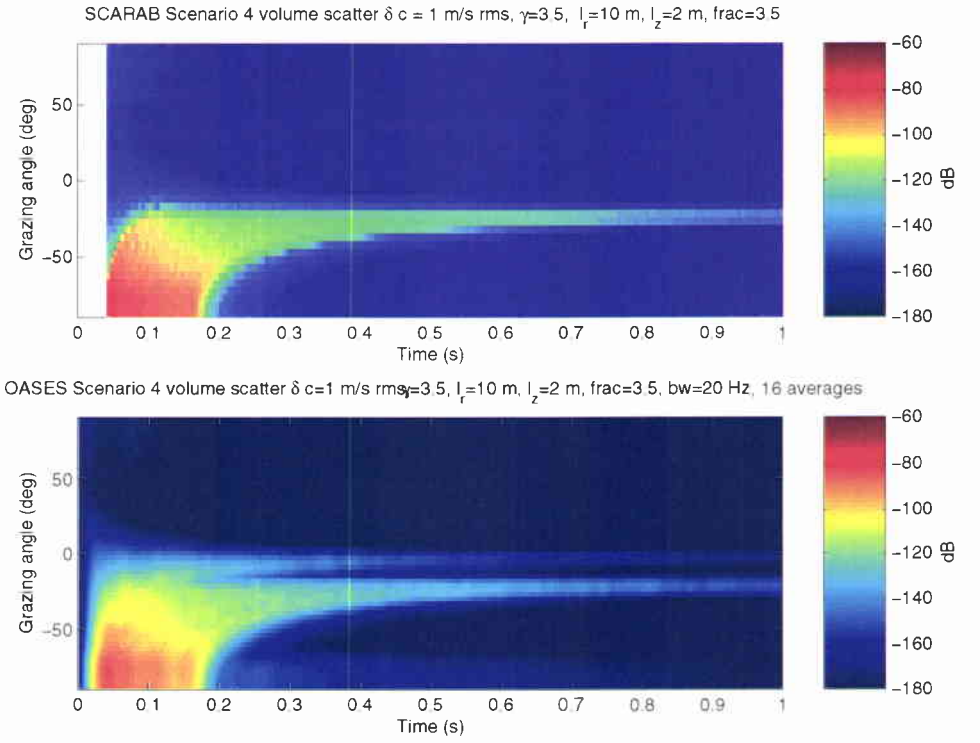

Figure 25 *Case 4, $\gamma = 3.5$, Beam-time evolution of scattered field as predicted by SCARAB (top) and OASES (bottom.) Again the shallow scattering branch associated with forced evanescent scattering is seen in the OASES results, as in Case 2.*

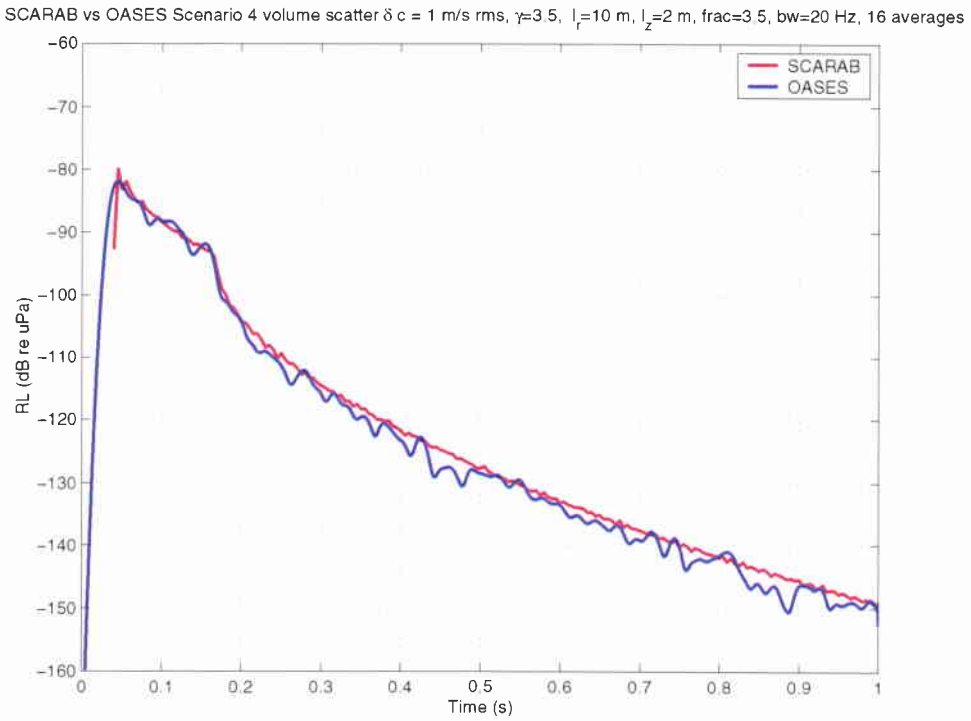

Figure 26 *Case 4, total scattered intensity as a function of time for a source/receiver combination deployed 25 m above the sediment-water interface. Predictions by SCARAB are shown in red and OASES in blue. As in Case 2, the agreement between OASES and SCARAB is very good even though SCARAB neglects the evanescent scattering branch.*

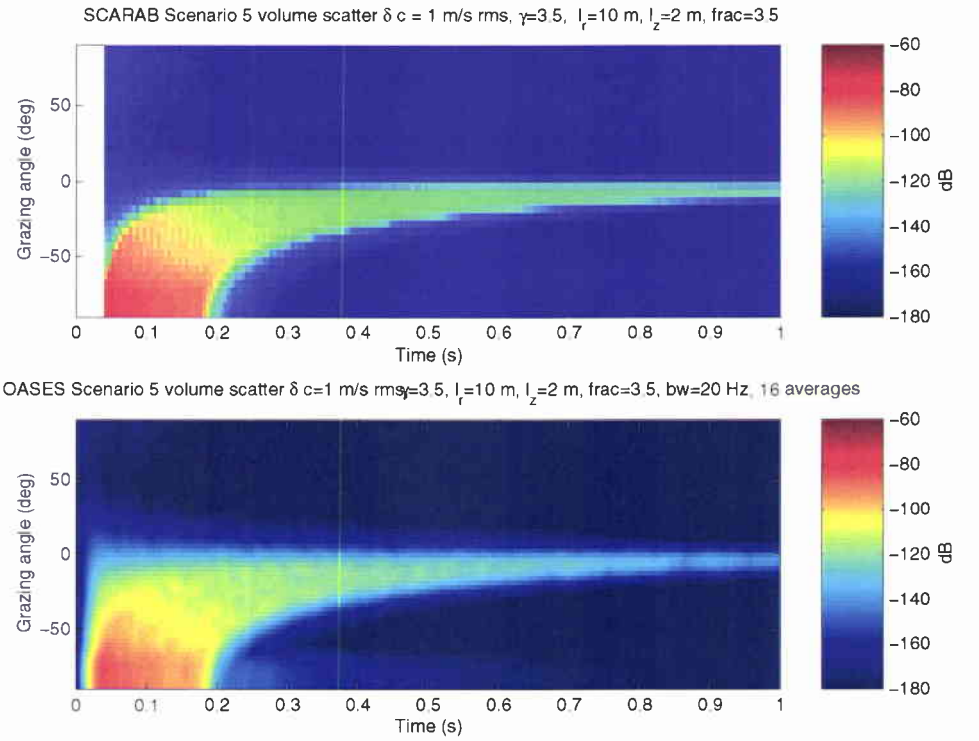

Figure 27 *Case 5, $\gamma = 3.5$, Beam-time evolution of scattered field as predicted by SCARAB (top) and OASES (bottom.)*

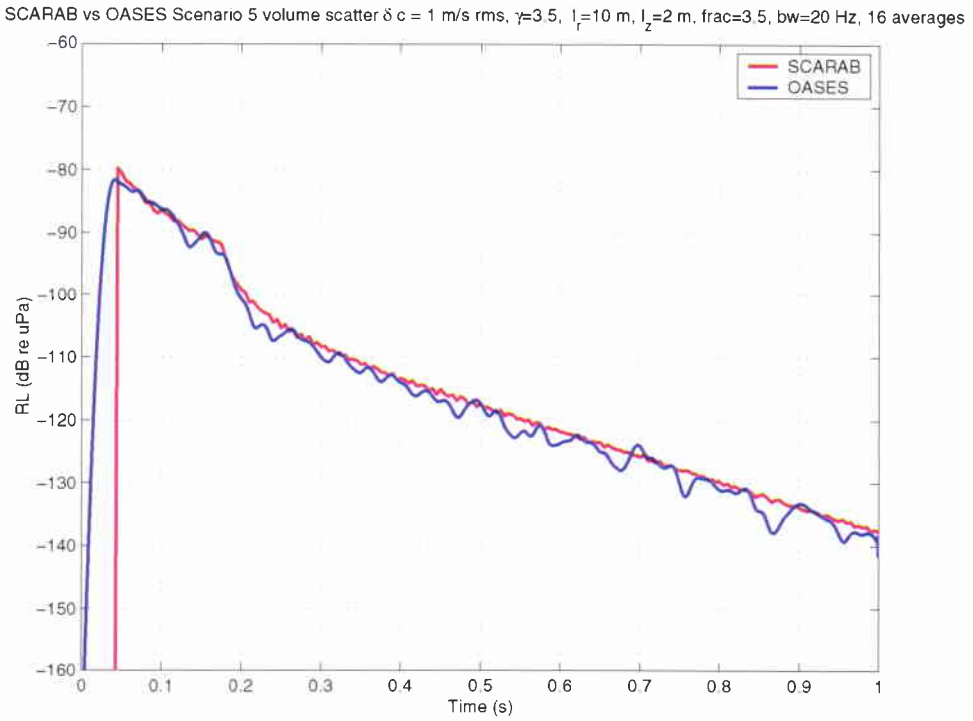

Figure 28 *Case 5, total scattered intensity as a function of time for a source/receiver combination deployed* 25 *m above the sediment-water interface. Predictions by SCARAB are shown in red and OASES in blue. OASES results have been ensemble averaged over* 16 *sediment scatterer realizations.*

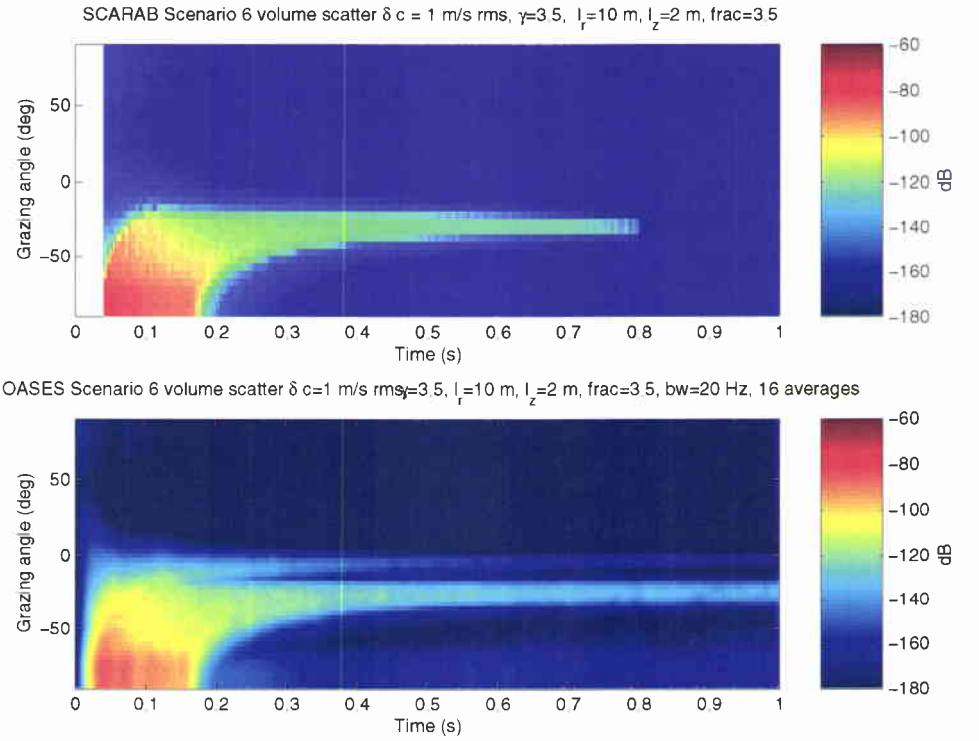

Figure 29 *Case 6, $\gamma = 3.5$, Beam-time evolution of scattered field as predicted by SCARAB (top) and OASES (bottom.) Here the deficiencies of SCARAB in including scattering from upward propagating rays is seen in the drop-off after about 0.8 s of the scattered returns. The OASES results show that backscattering continues beyond this time. SCARAB also neglects the very shallow scattering branch associated with evanescent ensonification of scatterers near the sediment-water interface.*

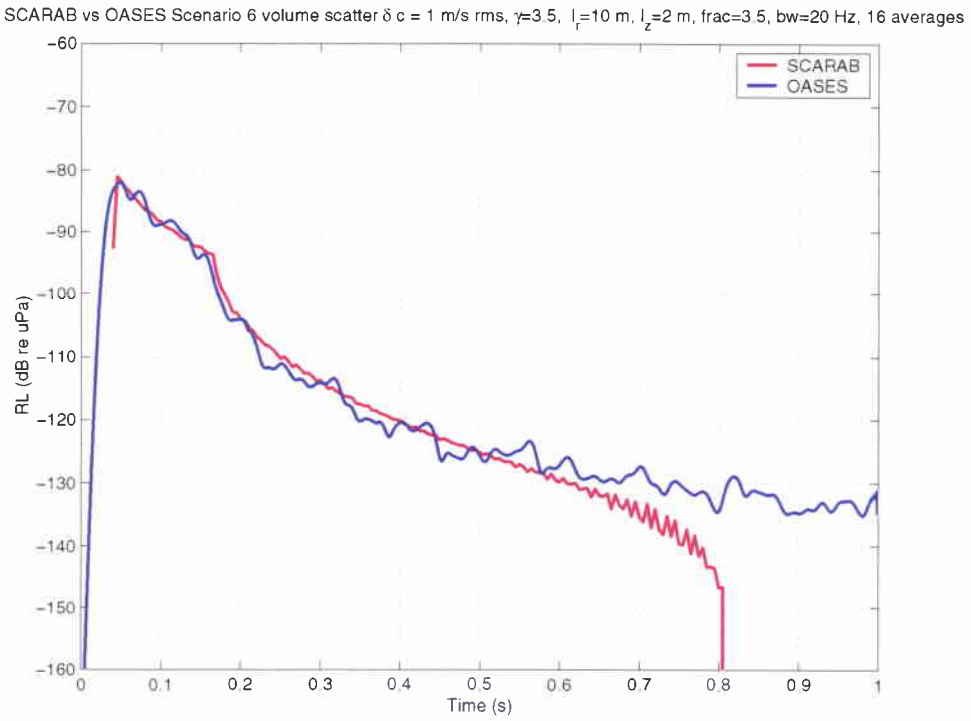

Figure 30 *Case 6, total scattered intensity as a function of time for a source/receiver combination deployed 25 m above the sediment-water interface. Predictions by SCARAB are shown in red and OASES in blue. The drop-off in the SCARAB intensity after 0.8 s is artificial and is caused by a problem with the incident field calculation, as discussed in Section 2.*

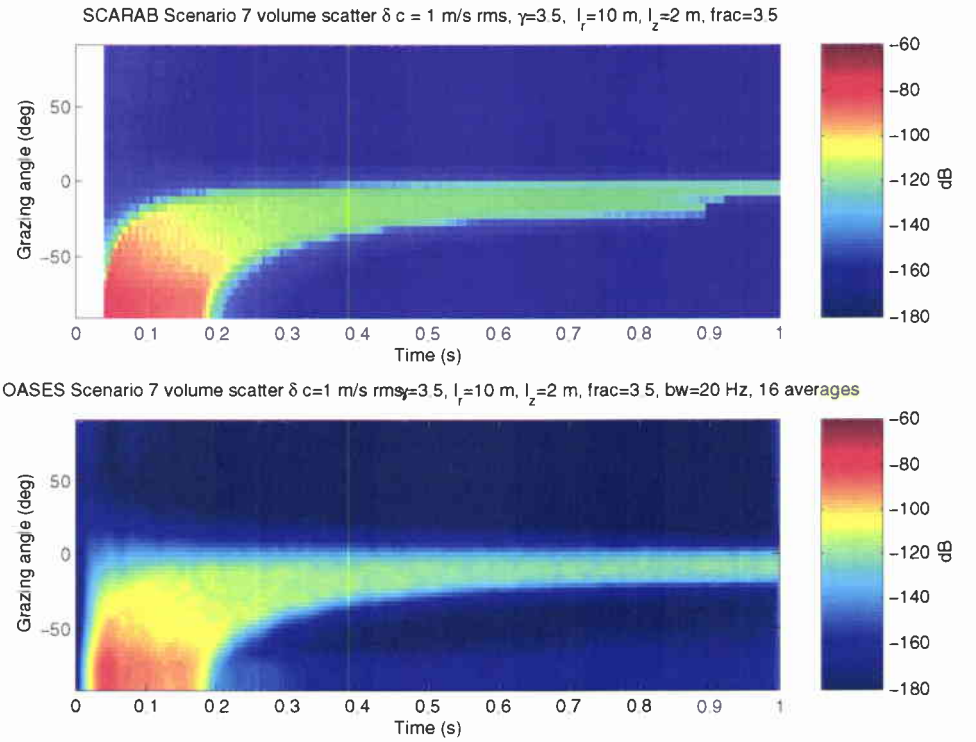

Figure 31 *Case 7, $\gamma = 3.5$, Beam-time evolution of scattered field as predicted by SCARAB (top) and OASES (bottom.) Problems are once again identified with the SCARAB solution at late time.*

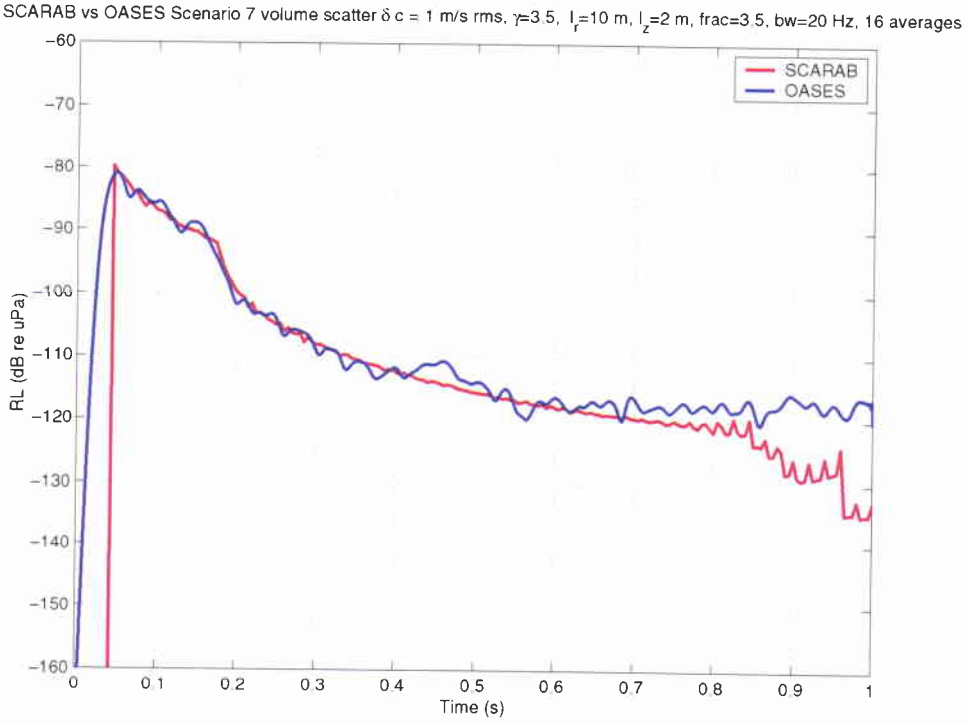

Figure 32 *Case 7, total scattered intensity as a function of time for a source/receiver combination deployed 25 m above the sediment-water interface. Predictions by SCARAB are shown in red and OASES in blue. Problems at late time are associated with the propagation engine in SCARAB.*

Report no. changed (Mar 2006): SM-377-UU

Document Data Sheet

Security Classification		Project No.
UNCLASSIFIED		04-D
Document Serial No.	**Date of Issue**	**Total Pages**
SM-377	March 2001	50 pp.

Author(s)

Bratberg, I., LePage, K., Holland, C., Schmidt, H.

Title

Benchmarking of SCARAB volume scattering versus OASES volume scattering

Abstract

OASES uses wavenumber integration to solve for the backscattered pressure caused by sound speed and density inhomogeneity scatterers in the sediment; SCARAB uses a ray path technique to find the backscattered intensity. This report compares the two models for a variety of sediment backscattering scenarios and identifies situations where the accuracy of SCARAB is compromised

Keywords

Issuing Organization

North Atlantic Treaty Organization
SACLANT Undersea Research Centre
Viale San Bartolomeo 400, 19138 La Spezia, Italy

[From N. America: SACLANTCEN (New York) APO AE 09613]

Tel: +39 0187 527 361
Fax:+39 0187 527 700

E-mail: library@saclantc.nato.int

The SACLANT Undersea Research Centre provides the Supreme Allied Commander Atlantic (SACLANT) with scientific and technical assistance under the terms of its NATO charter, which entered into force on 1 February 1963. Without prejudice to this main task - and under the policy direction of SACLANT - the Centre also renders scientific and technical assistance to the individual NATO nations.

SACLANT Undersea Research Centre
Viale San Bartolomeo 400
19138 San Bartolomeo (SP), Italy

tel: +39 0187 527 (1) or extension
fax: +39 0187 527 700

e-mail: library@saclantc.nato.int

NORTH ATLANTIC TREATY ORGANIZATION